Particle
& Particle Systems Characterization
www.particle-journal.com
www.MaterialsViews.com

Ab Initio Simulation of Charge Transfer at the Semiconductor Quantum Dot/TiO_2 Interface in Quantum Dot-Sensitized Solar Cells

Xukai Xin, Bo Li, Jaehan Jung, Young Jun Yoon, Rana Biswas, and Zhiqun Lin**

Quantum dot-sensitized solar cells (QDSSCs) have emerged as a promising solar architecture for next-generation solar cells. The QDSSCs exhibit a remarkably fast electron transfer from the quantum dot (QD) donor to the TiO_2 acceptor with size quantization properties of QDs that allows for the modulation of band energies to control photoresponse and photoconversion efficiency of solar cells. To understand the mechanisms that underpin this rapid charge transfer, the electronic properties of CdSe and PbSe QDs with different sizes on the TiO_2 substrate are simulated using a rigorous ab initio density functional method. This method capitalizes on localized orbital basis set, which is computationally less intensive. Quite intriguingly, a remarkable set of electron bridging states between QDs and TiO_2 occurring via the strong bonding between the conduction bands of QDs and TiO_2 is revealed. Such bridging states account for the fast adiabatic charge transfer from the QD donor to the TiO_2 acceptor, and may be a general feature for strongly coupled donor/acceptor systems. All the QDs/TiO_2 systems exhibit type II band alignments, with conduction band offsets that increase with the decrease in QD size. This facilitates the charge transfer from QDs donors to TiO_2 acceptors and explains the dependence of the increased charge transfer rate with the decreased QD size.

1. Introduction

Dye-sensitized solar cells (DSSCs) are among the most promising photovoltaic devices for low-cost light-to-energy conversion with relatively high efficiency (η = 12.3%).[1] Notably, although some dyes (e.g., black dye) have wide absorption spectrum, most of the sensitizing dyes absorb light with limited wavelength and cannot be readily tuned.[2] In stark contrast to most dyes, due to their quantum-confined nature, semiconductor quantum dots (QDs), such as CdE (E = S, Se) or lower bandgap PbE, possessing size tunable broad absorption from visible (e.g., CdE) to near-infrared (e.g., PbE) range, narrow symmetric emission, and resistance to photobleaching under low-oxygen environment,[3] are ideally suited for light harvesting and mimicking photosynthesis. Moreover, QDs open up new avenues to utilize hot electrons or generate multiple charge carriers with a single photon.[2c] Clearly, QDs carry many advantageous characteristics and have emerged as the building block for use in next-generation solar cells. Recently, QDs have been exploited as light-harvesting assemblies to yield QD-sensitized solar cells (QDSSCs).[2b-d,4] The ability to tailor optical and electrical properties of QDs by means of dimension (i.e., size and shape) and chemical composition (e.g., CdSe vs PbSe) offers the remarkable flexibility to tune the performance of QDSSCs.[5] In QDSSCs, the photons are absorbed by QDs, generating photoexcited carriers, which rapidly relax to the edges of conduction and valence bands. These photoexcited electrons are injected from QDs to the conduction band of photoanode composed of TiO_2 and the QDs are regenerated by the use of the redox couple (e.g., S^{2-}/S_n^{2-}).[2d]

Recently, transient absorption measurements on CdSe and CdTe QDs attached to TiO_2 nanoparticles revealed a very fast charge injection from QDs to TiO_2 on the picosecond time scale.[2b,5,6] The charge transfer rate increased for the smaller CdSe QDs, and was proportional to the driving force, i.e., the energy difference between the acceptor and donor.[5,6] The nonadiabatic Marcus mechanism of charge transfer was proposed to evaluate these observations.[6a] The smallest CdSe QDs with a diameter of 2.4 nm exhibited the highest transfer rates ($\approx 10^{10}$ s^{-1}; corresponding to ≈100 ps time scale).[6a] However, there was an incomplete understanding of such rapid charge injection process (i.e., the atomistic nature of charge injection).[6a] To this end, rigorous time-dependent methods for the ab initio charge dynamics have been invoked to study the charge injection from PbSe QDs to TiO_2,[7] in which the dynamics of the coupled electron and lattice systems was

Dr. X. Xin, B. Li, J. Jung, Y. J. Yoon, Prof. Z. Lin
School of Materials Science and Engineering
Georgia Institute of Technology
Atlanta, GA 30332, USA
E-mail: zhiqun.lin@mse.gatech.edu
Prof. R. Biswas
Department of Physics and Astronomy
and Ames Laboratory
U.S. Department of Energy
Iowa State University
Ames, IA 50011, USA
E-mail: biswasr@iastate.edu

DOI: 10.1002/ppsc.201400111

simulated over a period of >10 ps.[7] The simulation showed that the adiabatic charge transfer from PbSe QDs to TiO_2 was the dominant mechanism with a much smaller nonadiabatic or tunneling component.[7] Clearly, it is possible to explore the charge injection process with the adiabatic approach to increase the calculation efficiency while retaining the capability of achieving reliable results.

Here, we report on an approach based on adiabatic time-independent ab initio calculations to scrutinize the electronic states that participate in charge transfer at the QD/TiO_2 interface where no capping organic ligands are present at the QD surface. The simulation was performed on not only individual CdSe (both bulk and QD), PbSe (both bulk and QD), and TiO_2 (bulk) but also the CdSe QD/TiO_2 slab and PbSe QD/TiO_2 slab systems to study the charge injection process. In stark contrast to the plane wave approaches as in the copious past work,[7,8] this method capitalized on the localized orbital basis set that is computationally less intensive, with which many features, including electronic structure, density of states, and equilibrium lattice constants, are well described. A remarkable set of electron bridging states between the QDs (i.e., CdSe and PbSe) and the TiO_2 substrate was revealed. These states were occurred via the strong bonding between the conduction bands of QDs and TiO_2, thereby facilitating the fast adiabatic charge transfer from QDs to TiO_2. The present adiabatic time-independent ab initio calculations may be extended to interrogate other strongly coupled systems including organic donor/acceptor bulk heterojunction.

2. Theoretical Approach

In this work, the Spanish Initiative for Electronic Simulations with Thousands of Atoms (SIESTA)[9] method was employed to simulate the electronic properties at the interface of QDs and anatase TiO_2 substrate (i.e., CdSe/TiO_2 and PbSe/TiO_2) to elucidate the key features of the charge injection process. The wavefunction isosurface plots were used to further investigate the details of the coupling at the donor/acceptor interface. We note that previous time-independent density functional simulations were centered on the electrical and optical properties of CdSe,[8c,10] PbSe,[8b,8c,11] and TiO_2 solely.[12] The interaction between CdSe QDs and TiO_2 substrate has not yet been investigated.

The ab initio density functional theory (DFT)[13] with the SIESTA[9] method utilized the Perdew–Burke–Ernzerhof (PBE) exchange-correlation functional[14] based on the general gradient approximations (GGA) to treat the nonlocal exchange and correlation energies. 4d states of Cd and 5d states of Pb were included when calculating Cd and Pb atoms. We also utilized the PBE-solid (PBE-SOL) exchange-correlation functional[15] and the local density approximation (LDA) to obtain electronic structure, density of states, and equilibrium lattice constants of bulk anatase TiO_2, wurtzite CdSe, and cubic PbSe for comparison with those calculated by PBE and GGA, respectively. Moreover, bulk TiO_2, CdSe, and PbSe were also simulated and compared with previous work in literature[10b,16] to verify the accuracy of the simulation. Subsequently, the small QDs (Cd_6Se_6 and Pb_4Se_4) were simulated, followed by larger ones ($Cd_{36}Se_{36}$ and $Pb_{68}Se_{68}$). The temperature is set at 0 K for the simulations, to investigate ground-state properties.

The stoichiometric anatase TiO_2 (101) surface was modeled with a periodic slab as most of available anatase TiO_2 crystals are dominated by the thermodynamically stable (101) facets (>94%; according to the Wulff construction).[12b,17] A 288 atom system ($4 \times 6 \times 2$) with 4, 6, and 2 unit cells (each unit cell contains six atoms) in x, y, and z directions was simulated. A vacuum region of 3 nm was inserted between the slab and its periodic image along the z direction for the insertion of QDs later as this region is large enough to accommodate the largest QD calculated (≈1.8 nm). Periodic boundary conditions were used in the x and y directions. The $Cd_{36}Se_{36}$ (≈1.6 nm) and $Pb_{68}Se_{68}$ (≈1.8 nm) QDs were deposited on the anatase TiO_2 slab surface. Within this geometry, the QDs were separated by more than 1 nm from their periodic images in the x and y directions, thereby being electronically isolated from their images. The size of simulated $Cd_{36}Se_{36}$ QD (≈1.6 nm) and $Pb_{68}Se_{68}$ QD (≈1.8 nm) were comparable to those used in the experimental study (≈2.4 nm).[6a] The simulations signified that computationally efficient local-orbital-based approach can be an effective alternative to plane-wave-based approaches for studying inorganic systems including the charge transfer process.

3. Results and Discussion

Bulk structures of anatase TiO_2, wurtzite CdSe, and cubic PbSe were simulated with the DFT approach using the first-principles SIESTA technique. The calculated lattice constants for TiO_2, CdSe, and PbSe agreed well with experimental values[10–12] within 2% of errors (Table S1, Supporting Information), suggesting that our simulation correlated well with experimental data on the bulk reference systems. The calculated electronic density of states (DOS) and electronic band structures (**Figure 1**) yielded the bandgaps, E_g of bulk anatase TiO_2, wurtzite CdSe, and cubic PbSe of $E_{g,TiO2}$ = 2.83 eV, $E_{g,CdSe}$ = 1.57 eV, and $E_{g,PbSe}$= 0.51 eV, respectively; while the experimental values of these bulk materials are $E_{g,TiO2}$ = 3.20, $E_{g,CdSe}$ = 1.74, and $E_{g,PbSe}$ = 0.27 eV, respectively.[10–12] This is not surprising as it is well known that the DFT tends to underestimate the bandgap.[18] The electronic band structure of CdSe and PbSe showed a direct bandgap at Γ and L points, respectively (Figure 1e,f). The electronic band structure for anatase TiO_2 showed both a direct bandgap of 2.60 eV at Γ point and a higher indirect bandgap of 2.83 eV between Γ point and M point (Figure 1d). The 0.23 eV difference of these bandgaps (i.e., 2.83–2.60 = 0.23 eV) was consistent with previous simulation results.[16b] CdSe and PbSe QDs of different size were simulated. **Figure 2**a shows the DOS spectra of bulk CdSe, Cd_6Se_6 QD, and $Cd_{36}Se_{36}$ QD. The positions of atoms in Cd_6Se_6 and $Cd_{36}Se_{36}$ QDs after relaxation are illustrated in Figure 2b,c. From the DOS spectra, the bandgaps of Cd_6Se_6 QD, $Cd_{36}Se_{36}$ QD, and bulk CdSe were found to be 1.93, 1.72, and 1.57 eV, respectively. Clearly, as the QD size decreased, the bandgap increased, as expected due to the quantum confinement effect. The formation energy per atom, E_{form} decreased as the size of QDs increased, i.e., $E_{form,Cd6Se6}$ = 0.72 eV for Cd_6Se_6 and $E_{form,Cd36Se36}$ = 0.43 eV for $Cd_{36}Se_{36}$, respectively. The smaller QDs have larger surface to volume ratio, leading to a larger surface energy, and thus higher energy per atom.

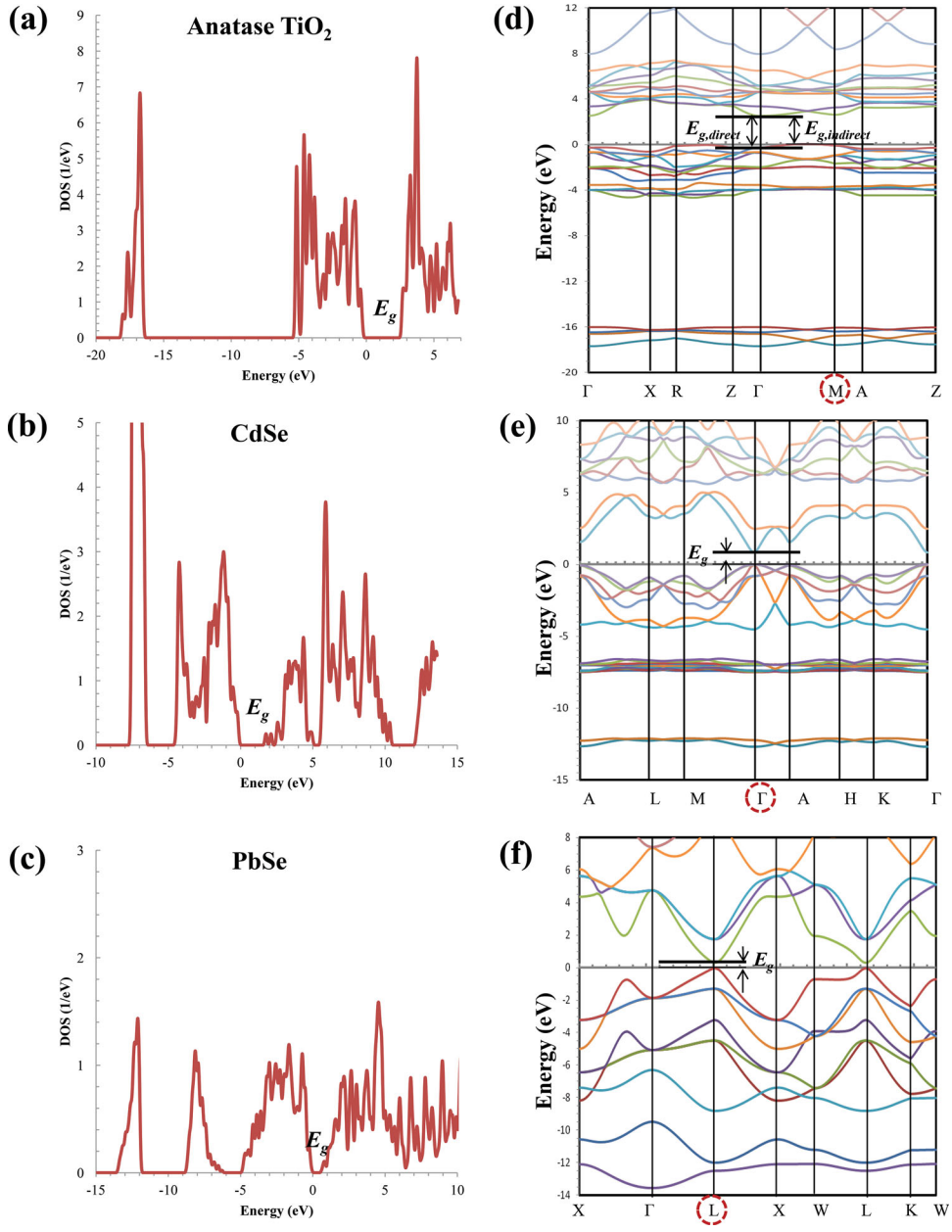

Figure 1. DOS spectra of bulk a) TiO_2, b) CdSe, and c) PbSe, and the corresponding electronic band structures of d) TiO_2, e) CdSe, and f) PbSe.

For PbSe QDs, a similar analysis was performed with different numbers of Pb and Se atoms, as PbSe has a cubic structure and is different from the wurtzite CdSe. The DOS spectra of bulk PbSe, Pb_4Se_4 QD, and $Pb_{68}Se_{68}$ QD are shown in **Figure 3**a. The positions of atoms in Pb_4Se_4 and $Pb_{68}Se_{68}$ QDs after relaxation are depicted in Figure 3b,c, respectively. Similar to the case of CdSe QDs noted above, the bandgaps of Pb_4Se_4 QD, $Pb_{68}Se_{68}$ QD, and bulk PbSe were 2.52, 0.70, and 0.51 eV, respectively. The formation energy per atom for Pb_4Se_4, $E_{form,Pb4Se4}$ = 0.64 eV, and for $Pb_{68}Se_{68}$, $E_{form,Pb4Se4}$ = 0.29 eV. In order to visualize the electron states in CdSe and PbSe QDs, the wavefunction isosurface plots of the conduction band and valence band for CdSe and PbSe QDs were constructed using a 3-nm supercell cube, which was large enough to accommodate both Cd_6Se_6 and $Cd_{36}Se_{36}$ QDs in the present simulation (Figure S1, Supporting Information).

To explore the charge injection at the donor/acceptor interface, an anatase TiO_2 substrate was selected as the acceptor. An anatase TiO_2 slab with 288 atoms was simulated (Figure S2, Supporting Information) with an exposed (101) surface, which is the most stable surface of anatase TiO_2. The periodic boundary conditions were applied in the x and y directions. Recently, it was shown that the ligands can have profound effect on the injection dynamics,[19] and the morphology of the metal oxide influences the injection dynamics.[20] However, to simplify the simulation and focus on the key interfacial properties, QDs

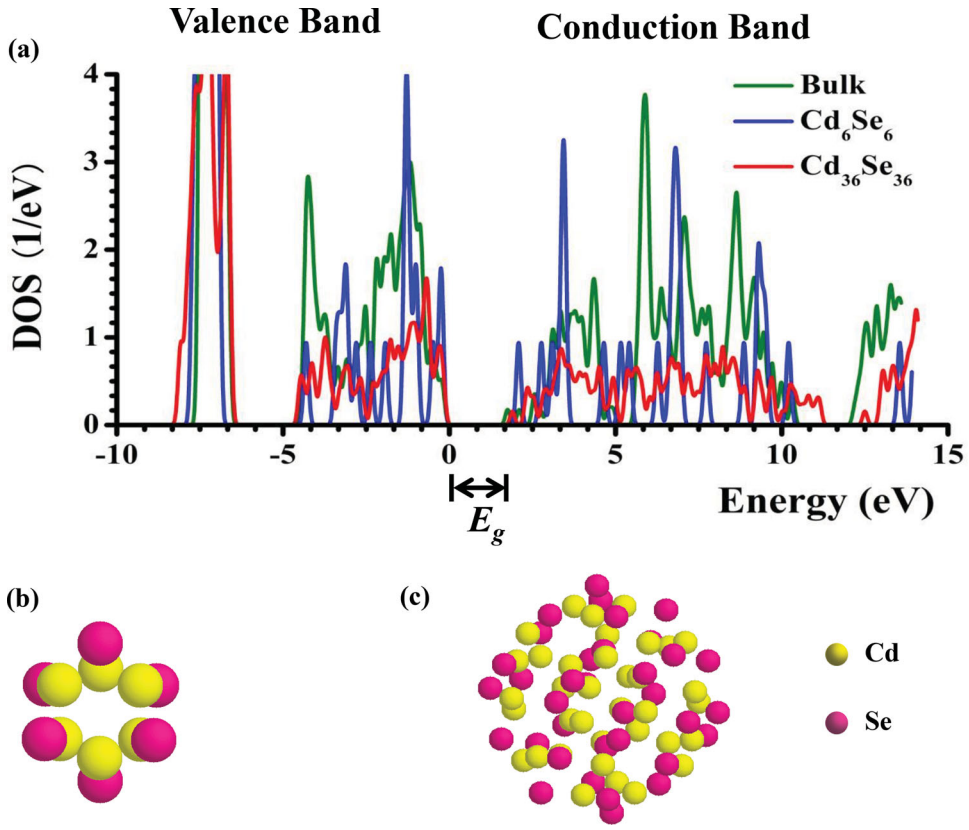

Figure 2. a) DOS spectra of bulk CdSe (olive curve), Cd_6Se_6 QD (blue curve), and $Cd_{36}Se_{36}$ QD (red curve). The positions of atoms in b) Cd_6Se_6 QD and c) $Cd_{36}Se_{36}$ QD, respectively. The yellow and magenta spheres represent Cd and Se atoms, respectively.

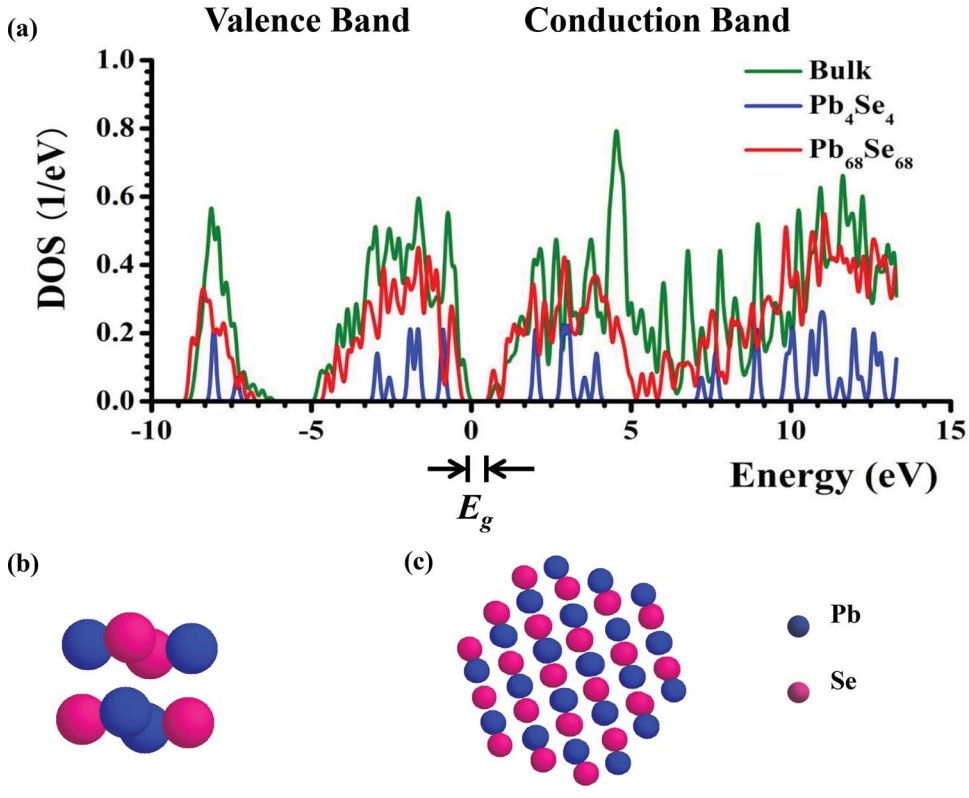

Figure 3. a) DOS spectra of bulk PbSe (olive curve), Pb_4Se_4 QD (blue curve), and $Pb_{68}Se_{68}$ QD (red curve). The positions of atoms in b) Pb_4Se_4 QD and c) $Pb_{68}Se_{68}$ QD, respectively. The blue and magenta spheres represent Pb and Se atoms, respectively.

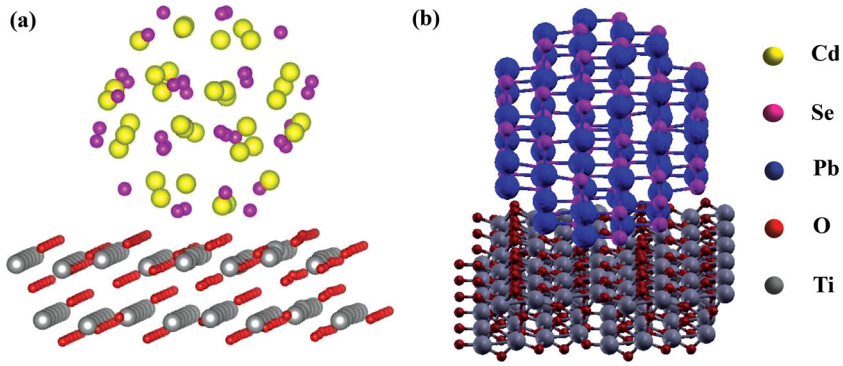

Figure 4. The geometry of a) anatase (101) with $Cd_{36}Se_{36}$ QD on its surface, and b) anatase (101) with $Pb_{68}Se_{68}$ QD on its surface. The yellow, blue, and magenta spheres represent Cd, Pb, and Se atoms, respectively. The gray and red spheres refer to Ti and O atoms, respectively.

were placed in direct contact with anatase TiO_2 (101) surface without any passivating ligands on the QD surface. Such intimate contact between QD and TiO_2 is advantageous for charge transfer and is experimentally possible by successive ionic layer adsorption and reaction (SILAR) processes.[21] **Figure 4** illustrates the geometry of relaxed anatase (101) with (a) $Cd_{36}Se_{36}$ and (b) $Pb_{68}Se_{68}$ QDs, respectively. The atomic positions of these QD/TiO_2 systems were fully relaxed. The binding energy of the QD/TiO_2 system, E_{bind}, can be given as

$$E_{bind} = E_{QD/TiO_2} - E_{TiO_2} - E_{QD} \quad (1)$$

where $E_{QD/TiO2}$ is the total energy of the relaxed QD/TiO_2 systems, and E_{TiO2} and E_{QD} are the energy of TiO_2 substrate and QD solely, respectively. For the $Cd_{36}Se_{36}$/TiO_2 system, the binding energy was $E_{bind,Cd36Se36/TiO2}$ = 4.2 eV, while $E_{bind,Pb68Se68/TiO2}$ = 6.4 eV for the $Pb_{68}Se_{68}/TiO_2$ system. The larger binding energy of $Pb_{68}Se_{68}$/TiO_2 system resulted from more chemical bonding between PbSe QD and TiO_2 than that between CdSe QD and TiO_2.

Figure 5a shows the electronic DOS of the TiO_2 substrate, $Cd_{36}Se_{36}$ QD, and $Cd_{36}Se_{36}$/TiO_2 system. The energies of the states relative to the Fermi energy E_f, were indicated with the numbers of 1–18 in Figure 5b. There are no electronic states in the bandgap suggesting that interfacial defects are not formed. Dangling bond[22] may be eliminated by relaxation of the local bonding. To further elucidate the interfacial properties, electron wavefunction isosurface plots of several representative electron states were calculated and illustrated in **Figure 6**, and the large set of wavefunctions was plotted in Figure S3 (Supporting Information) inside a 3-nm supercell cube. Figure 6 displays the absolute value of the wavefunction of the highest valence band of the TiO_2 substrate (upper left panel; marked as 4 in Figure 6), the highest valence band of the $Cd_{36}Se_{36}$ QD (upper right panel; marked as 9 in Figure 6), the lowest conduction band of the TiO_2 substrate (lower left panel; marked as 10 in Figure 6), and the lowest conduction band of the $Cd_{36}Se_{36}$ QD (lower right panel; marked as 14 in Figure 6). A complete set of wavefunctions was shown in Figure S3 (Supporting Information) and discussed in the Supporting Information. Quite intriguingly,

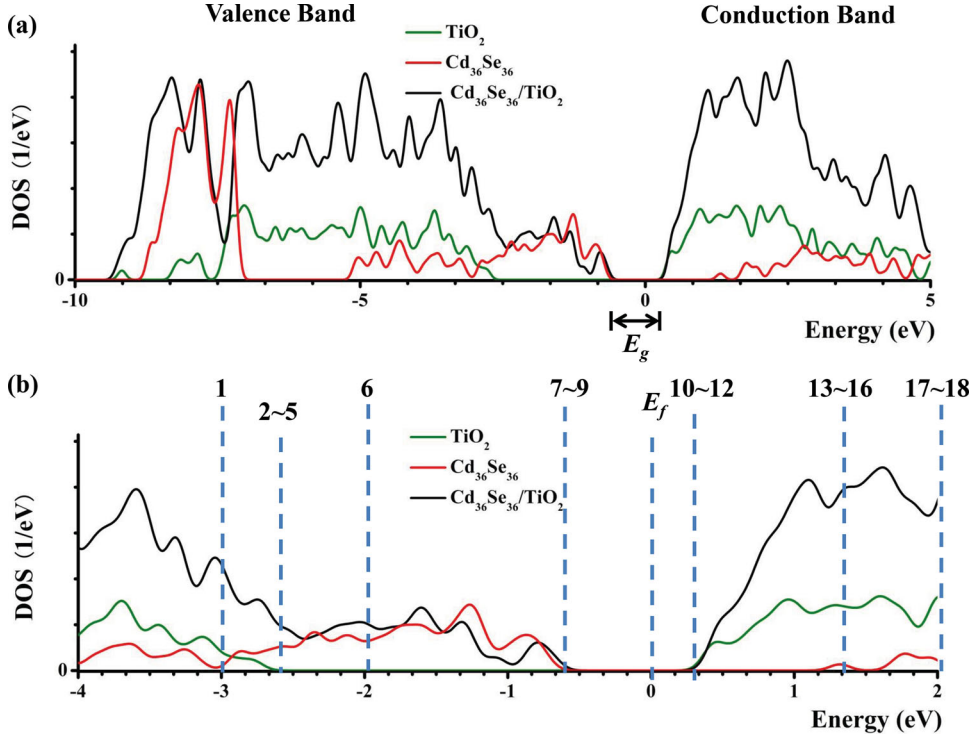

Figure 5. a) DOS spectra for the TiO_2 substrate (olive), $Cd_{36}Se_{36}$ QD (red), and $Cd_{36}Se_{36}/TiO_2$ system (black). b) The close-up of DOS spectra near the Fermi energy, E_f. The numbers 1 to 18 corresponded to the number of wavefunction plots in Figure S3 (Supporting Information).

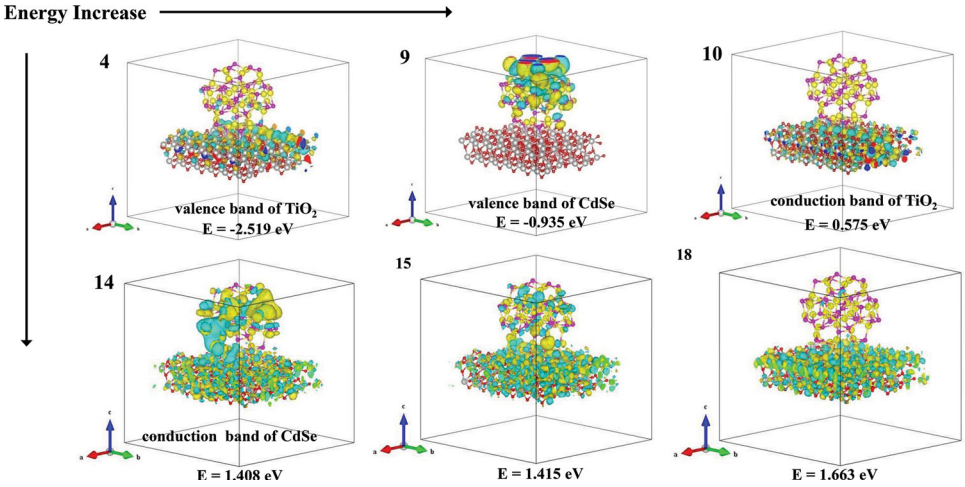

Figure 6. Wavefunction isosurface plots for the $Cd_{36}Se_{36}/TiO_2$ system. The energies of the states relative to the Fermi energy (E_f) were indicated with the numbers (i.e., 4, 9, 10, 14, 15, and 18). The energy value relative to E_f for each state was also given in the figure.

the state at the lowest conduction band of $Cd_{36}Se_{36}$ (i.e., plot 14 in Figure 6) exhibited a very strong overlap between the wavefunctions of the $Cd_{36}Se_{36}$ QD and the TiO_2 substrate. This plot clearly showed a bridging state wavefunction between the $Cd_{36}Se_{36}$ donor and the TiO_2 acceptor, signifying that the charge transfer from $Cd_{36}Se_{36}$ to TiO_2 can be greatly facilitated through this bridging state. The bridging state we found may be related to recent experimental findings, which revealed the existence of charge transfer states (CTS) between QDs and metal oxides.[23] Upon the absorption of photons, the electrons of $Cd_{36}Se_{36}$ were first excited from the ground state (i.e., plot 9 in Figure 6) to an excited state above the lowest conduction band (i.e., plot 14 in Figure 6). The electrons rapidly relaxed to the lowest CdSe conduction band (i.e., plot 14) due to the strong electron-phonon coupling.[26] Owing to the presence of bridging wavefunctions between $Cd_{36}Se_{36}$ and TiO_2, the excited electrons can then transfer adiabatically from the $Cd_{36}Se_{36}$ QD to the TiO_2 substrate (i.e., plot 14) and relax to several lower energy states localized on the TiO_2 substrate (i.e., plots 10). Thus, the charge injection from the $Cd_{36}Se_{36}$ QD to TiO_2 substrate primarily involved a smooth crossing from the electron energy surface of QDs to the electron energy surface of TiO_2 with no quantum jump occurring (i.e., adiabatic electron motion), which was consistent with the time-dependent DFT calculations,[7,8] as the latter found that the adiabatic contribution dominated over the nonadiabatic charge transfer for the PbSe QD/TiO_2 system.

In addition to the $Cd_{36}Se_{36}/TiO_2$ system, the simulation was also performed on PbSe QDs on TiO_2 substrates. Recently, PbSe QDs have been shown to generate multiple excitons from a single photon of sufficient energy,[24] thereby offering the possibility of increasing the photocurrent to enhance power conversion efficiency.[24d] The carrier multiplication efficiency of 1.7 has been observed for excitation near 4.8 times the bandgap for the low bandgap PbSe nanocrystals.[25] The electronic DOS spectra of the anatase TiO_2 substrate, $Pb_{68}Se_{68}$ QD, and $Pb_{68}Se_{68}/TiO_2$ system are shown in **Figure 7**a. The numbers of 1–18 in Figure 7b marked the energies of the states relative to E_f. Similar to the case of the $Cd_{36}Se_{36}/TiO_2$ system, the representative and a full set of electron wavefunction isosurface plots within a 3-nm supercell cube were displayed in **Figure 8** and Figure S4 (Supporting Information), respectively. The wavefunctions for the

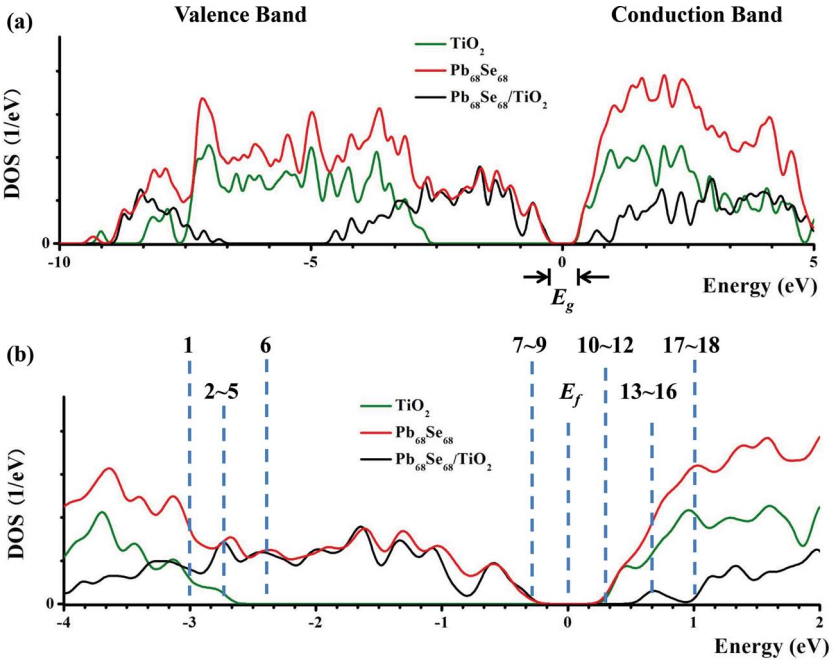

Figure 7. a) DOS spectra for the TiO_2 substrate (olive), $Pb_{68}Se_{68}$ QD (red), and $Pb_{68}Se_{68}/TiO_2$ system (black). b) The close-up of DOS spectra near E_f. The numbers 1 to 18 corresponded to the number of wavefunction plots in Figure S4 (Supporting Information).

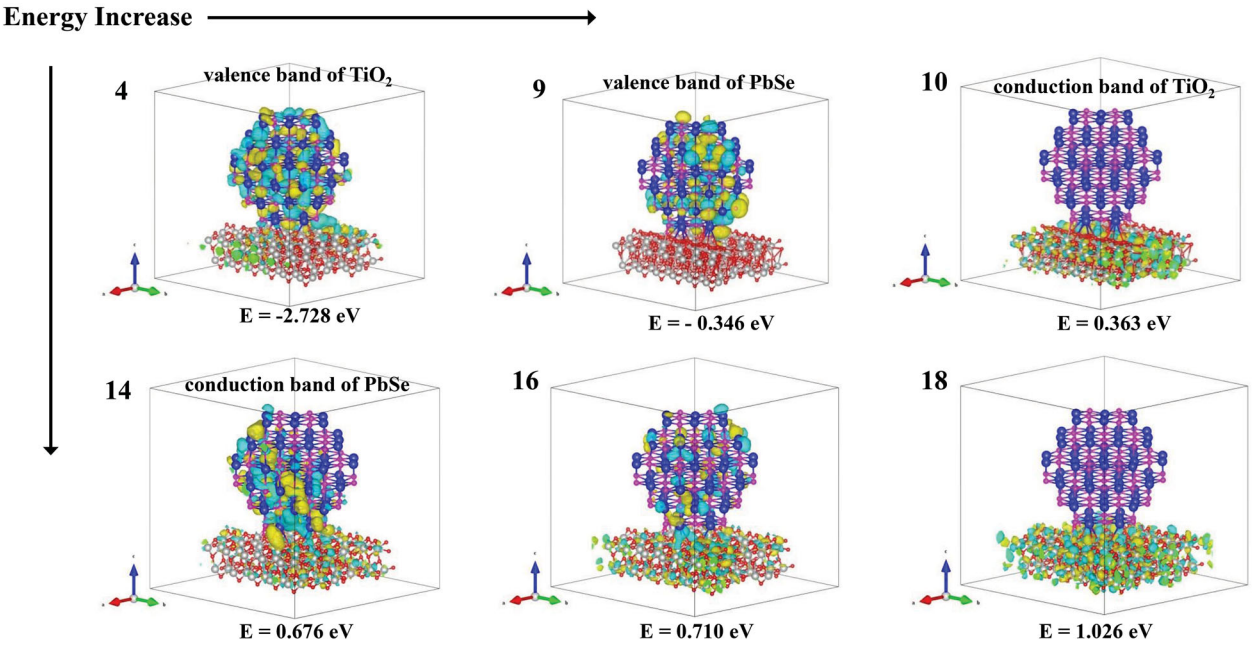

Figure 8. Wavefunction isosurface plots for the $Pb_{68}Se_{68}/TiO_2$ system. The energies of the states relative to E_f were marked with the numbers (i.e., 4, 9, 10, 14, 16, and 18). The energy value relative to E_f for each state was also given in the figure.

electron states at the highest valence band of the TiO_2 substrate (i.e., plot 4), the highest value of valence band of $Pb_{68}Se_{68}$ QD (i.e., plot 9), the lowest conduction band of the TiO_2 substrate (i.e., plot 10), and the lowest conduction band of $Pb_{68}Se_{68}$ QD (i.e., state 14) are illustrated in Figure 8 and discussed in the Supporting Information.

Similarly, a markedly bonded state between the $Pb_{68}Se_{68}$ QD and TiO_2 (i.e., a significant overlap between the wavefunctions of the $Pb_{68}Se_{68}$ QD and TiO_2 substrate) was located at the lowest $Pb_{68}Se_{68}$ conduction band (i.e., plot 14 in Figure 8). Thus, the charge transfer from the $Pb_{68}Se_{68}$ QD to TiO_2 substrate can occur adiabatically as a direct consequence of strong coupling of electronic states between the $Pb_{68}Se_{68}$ QD and TiO_2, resembling the charge transfer process from the $Cd_{36}Se_{36}$ QD to TiO_2 substrate discussed above. The photoexcited electrons in the $Pb_{68}Se_{68}$ QD at the excited state (i.e., plot 14 in Figure 8) can be easily injected to the TiO_2 substrate through the intimate bridging state and subsequently relaxed to the states with lower energy localized on the TiO_2 substrate [i.e., plots 10 to 13 in Figure S4 (Supporting Information)].

To explore the size dependence of the electron bridging states of QD/TiO_2 systems, smaller sized QDs (Cd_6Se_6, Pb_4Se_4, and $Pb_{16}Se_{16}$) on TiO_2 substrates were also simulated. The DOS and wavefunction plots are shown in **Figures 9–11**, respectively.

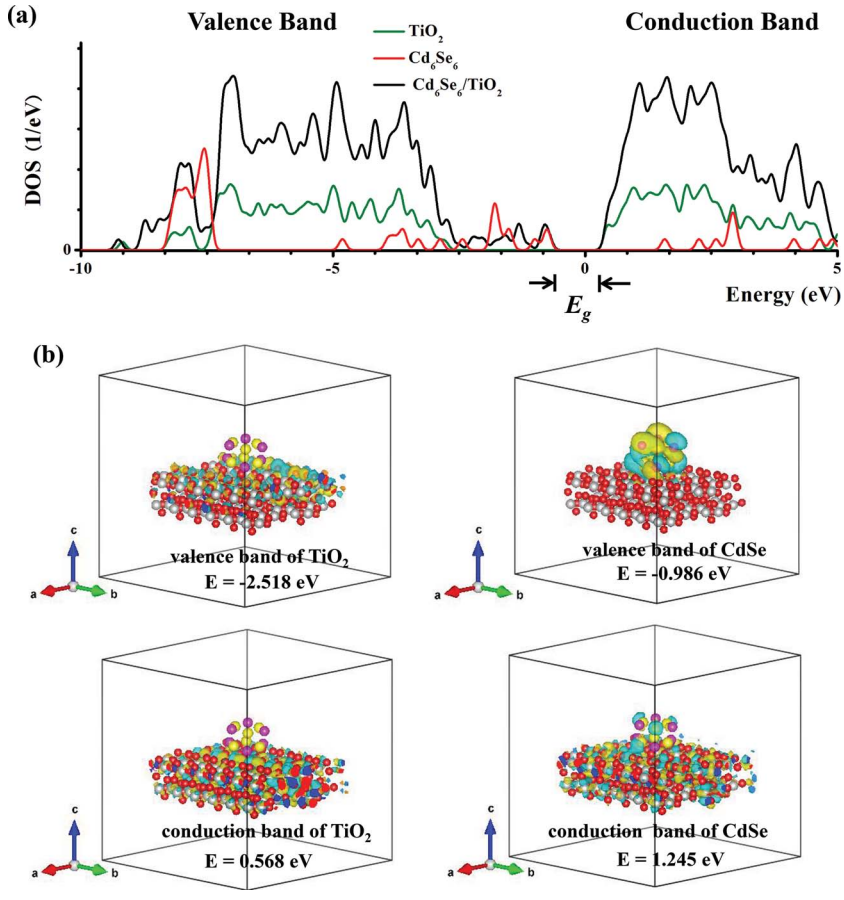

Figure 9. a) DOS spectra for the TiO_2 substrate (olive), Cd_6Se_6 QD (red), and Cd_6Se_6/TiO_2 system (black). b) Wavefunction isosurface plots for the Cd_6Se_6/TiO_2 system. The energies of the states relative to the Fermi energy (E_f) were indicated with the numbers.

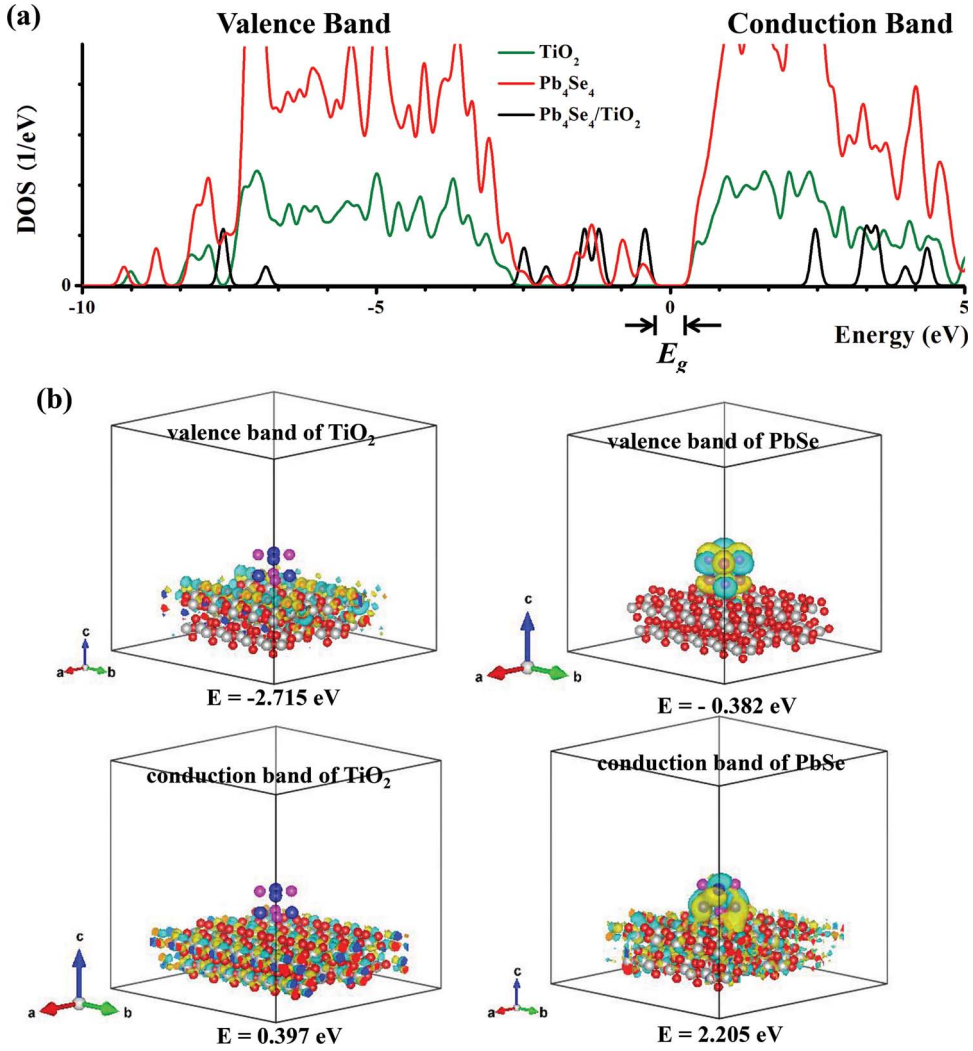

Figure 10. a) DOS spectra for the TiO_2 substrate (olive), Pb_4Se_4 QD (red), and Pb_4Se_4/TiO_2 system (black). b) The close-up of DOS spectra near E_f. The numbers 1 to 18 corresponded to the number of wavefunction plots in Figure S4 (Supporting Information).

Conduction band wavefunctions of all CdSe and PbSe QDs on TiO_2 (Figures 9b, 10b, and 11b) showed electron bridging states, which are likely common for all QD/TiO_2 systems.

It is worth noting that, recently, the strong bridging electronic states have also been found at the interface between poly-3-hexylthiophene (P3HT) and carbon nanotubes[26] (or phenyl-C_{61}-butyric acid methyl ester (PCBM))[27] in simulations, and account for the rapid charge transfer from the P3HT donor and the acceptor (e.g., PCBM) in organic photovoltaics, reflecting that such bridging electronic states may be a general feature in the heterogeneous donor/acceptor photovoltaic systems that exhibit rapid charge transfer.

By utilizing the calculated DOS of Cd_6Se_6/TiO_2 (Figure 9a), $Cd_{36}Se_{36}/TiO_2$ (Figure 5a), Pb_4Se_4/TiO_2 (Figure 10a), $Pb_{16}Se_{16}/TiO_2$ (Figure 11a), and $Pb_{68}Se_{68}/TiO_2$ (Figure 7) systems, their respective band alignments can be constructed (**Figure 12**). The energy band alignments in all QDs/TiO_2 systems were type II with the bottom of the QD conduction band above the bottom of the TiO_2 conduction band. This facilitated the electron transfer and prohibited the hole transfer from QDs to TiO_2, i.e., promoted the charge separation in QDs. Fluorescence resonance energy transfer (FRET) is the other possible transfer mechanism in solar cells,[28] which usually occurs when the emission spectrum of donors overlaps with the absorption spectrum of acceptors. Thus, the bandgap of the donor should be larger than the acceptor. However, in our study the QD donor had substantially smaller bandgaps than the TiO_2 acceptor. Therefore, the resonant energy transfer may be suppressed and charge transfer would dominate the transfer process. In addition, recent work by Pullerits and co-workers[29] suggested that the FRET in QD/metal oxide systems has a transfer time of 1.5 to 2 ns, which is too slow to interfere with the charge injection. The conduction band offsets between QD and TiO_2 were 1.20 eV for Cd_6Se_6 QD, 1.01 eV for $Cd_{36}Se_{36}$ QD, 2.02 eV for Pb_4Se_4 QD, 0.99 eV for $Pb_{16}Se_{16}$ QD, and 0.33 eV for $Pb_{68}Se_{68}$ QD, respectively. Clearly, the decrease of QD size increased the bandgap of QDs, and also increased the conduction band offsets between QDs and TiO_2. Compared with the large shifts of

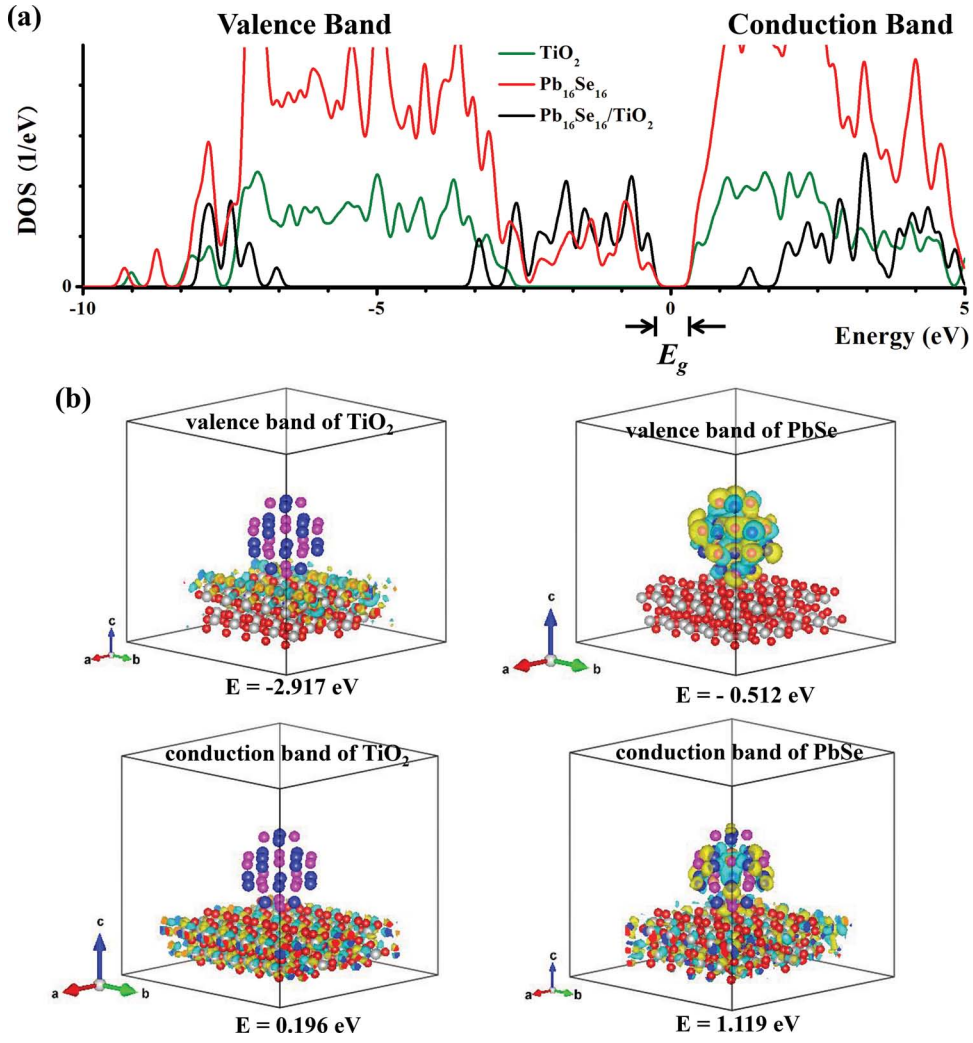

Figure 11. a) DOS spectra for the TiO_2 substrate (olive), $Pb_{16}Se_{16}$ QD (red), and $Pb_{16}Se_{16}/TiO_2$ system (black). b) Wavefunction isosurface plots for the $Pb_{16}Se_{16}/TiO_2$ system. The energies of the states relative to the Fermi energy (E_f) were indicated with the numbers.

conduction band offsets with QD size, the changes of valence band offsets were relatively small. In the case of CdSe QDs, the shift of valence band offsets was only 0.02 eV between Cd_6Se_6 QD and $Cd_{36}Se_{36}$ QD, 0.09 eV between Pb_4Se_4 QD and $Pb_{16}Se_{16}$ QD, and 0.04 eV between $Pb_{16}Se_{16}$ QD and $Pb_{68}Se_{68}$ QD, respectively. The small valence band shifts were consistent with previously reported values in the literature.[5,6]

Both CdSe and PbSe QDs inject the excited electrons into TiO_2, however, their injection rates may be different. The charge transfer rate from CdSe QDs to TiO_2[5,6] measured using the transient recovery of the photo-bleaching spectrum[5,6] was found to be much faster for small CdSe QD (D = 2.4 nm; K_{ET} = 10^{11} s^{-1}) than for larger one (D = 7.5 nm; K_{ET} = 10^7 s^{-1}), and explained with the nonadiabatic Marcus theory, as due to the larger difference in the QD and TiO_2 conduction bands, leading to larger driving force for charge transfer in smaller QDs. The generalized Mulliken–Hush method[30] is a very successful theory to quantify the electron injection donor–acceptor system in organic solar cells. However, whether this method can be used in inorganic quantum dot system is still not clear. We note that although the results were observed from ligand-capped QDs/TiO_2, the backbone of capping ligand in experiments is typically the alkyl chain, which would not participate in the electron transfer. Therefore, the trend of the injection rate with and without capping ligands would be qualitatively the same. As illustrated in the electronic DOS (Figure 5), there was a much *higher* density of the conduction band states of TiO_2 adjacent to the conduction band of $Cd_{36}Se_{36}$ QD (Figure 5a) than that adjacent to the conduction band of $Pb_{68}Se_{68}$ QD (Figure 7a), which had smaller bandgap). This is due to the TiO_2 band edge DOS scaling as $(E - E_c)^{1/2}$, where E is the energy of the TiO_2 conduction band, and E_c is the lowest TiO_2 conduction band (Figure 12). In the adiabatic mechanism, this results in an increased charge transfer rate from the $Cd_{36}Se_{36}$ QD to TiO_2 as compared to that from the $Pb_{68}Se_{68}$ QD to TiO_2. For the same kind of QDs as the QD size decreased, type II band alignments persist and the conduction band offsets increased with the decrease in QD size (Figure 12). There was a much higher conduction band DOS adjacent to the conduction band minima of the QD for smaller QD size (Figures 9,10 and 11).

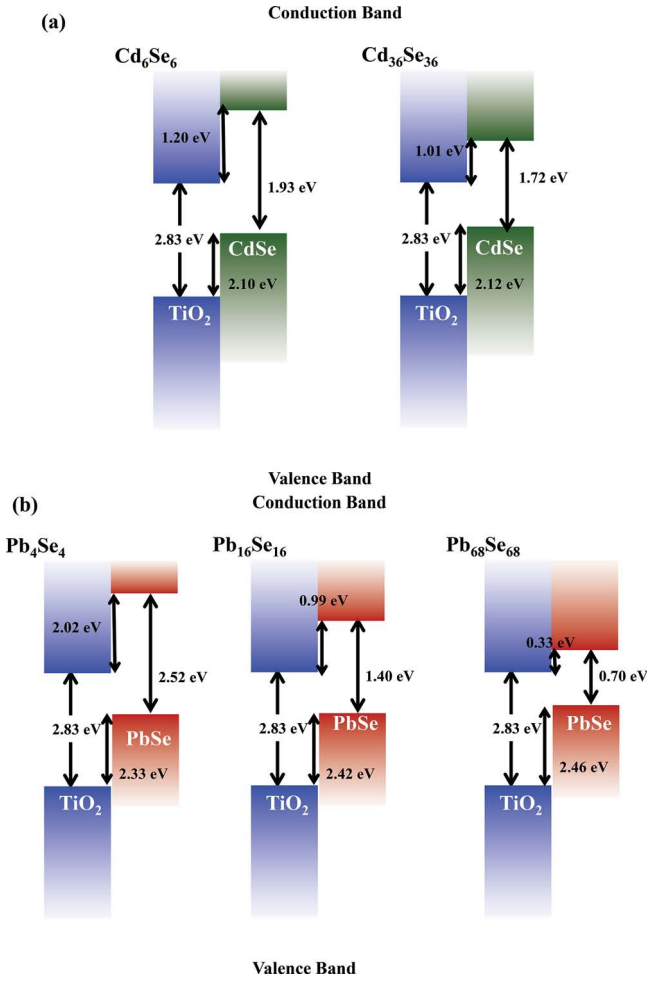

Figure 12. Schematic illustration of band alignments in a) $CdSe/TiO_2$, and b) $PbSe/TiO_2$ systems.

Thus, this mechanism (i.e., the larger the difference between the lowest conduction bands of QD and TiO_2, the faster charge transfer rate) also accounted for the higher charge transfer rate in smaller QDs, as reported in literature[2a-c,5,6,31] for CdSe. We note that ligands often employed to passivate QDs and prevent the aggregation of QDs, will hinder the occurrence of the strong donor/acceptor bridging states and may lead to a much slower charge transfer rates. The occurrence of the donor/acceptor bridging states through bonding overlaps between the donor QD orbitals and the acceptor TiO_2 orbitals is not prohibited by symmetry considerations. The strength of the donor/acceptor bridging states is controlled by the real-space distance-dependent overlap integrals between the donor and acceptor.

4. Conclusions

In summary, CdSe and PbSe QDs with different sizes on the anatase TiO_2 substrate were simulated using an ab initio local-orbital-based density functional approach. The formation energy, the bandgap, and the conduction band offsets of QDs increased as their size decreased. The isosurface wavefunction plots clearly revealed that the photoexcited charge injection from CdSe and PbSe QDs to TiO_2 was feasible through the bridging state. Quite intriguingly, a very strong bonding between the QDs (i.e., CdSe and PbSe) and the TiO_2 substrate were observed, represented as the bridging electronic states between the QD and TiO_2 substrate. Such bridging electronic states led to highly efficient adiabatic charge injection from QD and TiO_2, where the electron resides on a smooth energy surface. Importantly, the type II band alignments of the QD/TiO_2 systems suggested that charge injection rate from $Cd_{36}Se_{36}$ QD to TiO_2 was faster than that from $Pb_{68}Se_{68}$ QD to TiO_2. For the same kind of QDs, type II band alignments suggested faster electron injection rates as the QD size was decreased. While the computationally less intensive ab initio density functional method was introduced here to explore the charge transfer at the QD/TiO_2 interface, it can be easily extended to study the charge transfer in core/shell QD systems[32], and also at the other types of interface (e.g., organic/inorganic as in organic–inorganic hybrid solar cells) and provide valuable insight into high-efficiency solar cells, which is a subject of intense interdisciplinary research efforts.[31]

Supporting Information

Supporting Information is available from the Wiley Online Library or from the author.

Acknowledgements

This work was supported by the Air Force Office of Scientific Research (MURI FA9550-14-1-0037) (Z.L.), the Key Laboratory of Computational Physical Sciences at Fudan University, Shanghai, China (Z.L); and by the U.S. Department of Energy, Basic Energy Sciences, Materials Sciences and Engineering Division, under contract no. DE-AC 02–07CH11358 (R.B). This research used the resources of the National Energy Research Scientific Computing Center, which is supported by the Office of Science of the U.S. Department of Energy under contract no. DE-AC02–05CH11231.

Received: May 22, 2014
Published online: July 24, 2014

[1] a) B. O'Regan, M. Gratzel, *Nature* **1991**, *353*, 737; b) M. Ye, X. Xin, C. J. Lin, Z. Lin, *Nano Lett.* **2011**, *11*, 3214; c) X. Xin, M. He, W. Han, J. Jung, Z. Lin, *Angew. Chem Int. Ed.* **2011**, *50*, 11739; d) X. Xin, M. Scheiner, M. Ye, Z. Lin, *Langmuir* **2011**, *27*, 14594; e) X. Xin, J. Wang, W. Han, M. Ye, Z. Lin, *Nanoscale* **2012**, *4*, 964; f) M. Ye, H. Liu, C. Lin, Z. Lin, *Small* **2013**, *9*, 312; g) J. Wang, Z. Q. Lin, *Chem. Mater.* **2010**, *22*, 579.

[2] a) H. Choi, P. K. Santra, P. V. Kamat, *ACS Nano* **2012**, *6*, 5718; b) P. V. Kamat, *J. Phys. Chem. C* **2008**, *112*, 18737; c) P. V. Kamat, K. Tvrdy, D. R. Baker, J. G. Radich, *Chem. Rev.* **2010**, *110*, 6664; d) A. J. Nozik, M. C. Beard, J. M. Luther, M. Law, R. J. Ellingson, J. C. Johnson, *Chem. Rev.* **2010**, *110*, 6873.

[3] K. Žídek, K. Zheng, P. Chábera, M. Abdellah, T. Pullerits, *App. Phys. Lett.* **2012**, *100*, 243111.

[4] a) I. N. Mora-Seró, J. Bisquert, *J. Phys. Chem. Lett.* **2010**, *1*, 3046; b) I. J. Kramer, E. H. Sargent, *ACS Nano* **2011**, *5*, 8506.

[5] A. Kongkanand, K. Tvrdy, K. Takechi, M. Kuno, P. V. Kamat, *J. Am. Chem. Soc.* **2008**, *130*, 4007.
[6] a) I. Robel, M. Kuno, P. V. Kamat, *J. Am. Chem. Soc.* **2007**, *129*, 4136; b) K. Tvrdy, P. A. Frantsuzov, P. V. Kamat, *Proc. Natl. Acad. Sci.* **2011**, *108*, 29; c) P. V. Kamat, *Acc. Chem. Res.* **2012**; d) J. H. Bang, P. V. Kamat, *ACS Nano* **2009**, *3*, 1467; e) X.-Y. Yu, J.-Y. Liao, K.-Q. Qiu, D.-B. Kuang, C.-Y. Su, *ACS Nano* **2011**, *5*, 9494; f) X.-Y. Yu, B.-X. Lei, D.-B. Kuang, C.-Y. Su, *Chem. Sci.* **2011**, *2*, 1396.
[7] R. Long, O. V. Prezhdo, *J. Am. Chem. Soc.* **2011**, *133*, 19240.
[8] a) W. R. Duncan, O. V. Prezhdo, *Annu. Rev. Phys. Chem.* **2007**, *58*, 143; b) S. V. Kilina, C. F. Craig, D. S. Kilin, O. V. Prezhdo, *J. Phys. Chem. C* **2007**, *111*, 4871; c) S. V. Kilina, D. S. Kilin, O. V. Prezhdo, *ACS Nano* **2008**, *3*, 93.
[9] J. M. Soler, E. Artacho, J. D. Gale, A. Garcia, J. Junquera, P. Ordejon, D. Sanchez-Portal, *J. Phys. Condens. Matter* **2002**, *14*, 2745.
[10] a) J. Konior, J. Goniakowski, S. Kaprzyk, *J. Alloy. Compd.* **2001**, *328*, 139; b) O. Zakharov, A. Rubio, X. Blase, M. L. Cohen, S. G. Louie, *Phys. Rev. B: Condens. Matter* **1994**, *50*, 10780.
[11] N. L. Heda, A. Rathor, V. Sharma, G. Ahmed, Y. Sharma, B. L. Ahuja, *J. Alloy. Compd.* **2008**, *463*, 47.
[12] a) R. Asahi, Y. Taga, W. Mannstadt, A. J. Freeman, *Phys. Rev. B: Condens. Matter* **2000**, *61*, 7459; b) M. Lazzeri, A. Vittadini, A. Selloni, *Phys. Rev. B: Condens. Matter* **2001**, *63*, 155409.
[13] P. Hohenberg, W. Kohn, *Phys. Rev.* **1964**, *136*, B864.
[14] J. P. Perdew, M. Ernzerhof, K. Burke, *J. Chem. Phys.* **1996**, *105*, 9982.
[15] J. P. Perdew, A. Ruzsinszky, G. I. Csonka, O. A. Vydrov, G. E. Scuseria, L. A. Constantin, X. Zhou, K. Burke, *Phys. Rev. Lett.* **2008**, *100*, 136406.
[16] a) O. V. Prezhdo, *Acc. Chem. Res.* **2009**, *42*, 2005; b) S.-D. Mo, W. Y. Ching, *Phys. Rev. B: Condens. Matter* **1995**, *51*, 13023.
[17] H. G. Yang, C. H. Sun, S. Z. Qiao, J. Zou, G. Liu, S. C. Smith, H. M. Cheng, G. Q. Lu, *Nature* **2008**, *453*, 638.
[18] R. M. Dreizler, E. K. U. Gross, *Density Functional Theory: An Approach to the Quantum Many-Body Problem*, Springer, Berlin **1996**.
[19] T. Hansen, K. Žídek, K. Zheng, M. Abdellah, P. Chábera, P. Persson, T. Pullerits, *J. Phys. Chem. Lett.* **2014**, *5*, 1157.
[20] K. Zheng, K. Žídek, M. Abdellah, P. Chábera, M. S. Abd El-sadek, T. Pullerits, *App. Phys. Lett.* **2013**, *102*, 163119.
[21] a) H. Lee, M. Wang, P. Chen, D. R. Gamelin, S. M. Zakeeruddin, M. Grätzel, M. K. Nazeeruddin, *Nano Lett.* **2009**, *9*, 4221; b) H. J. Lee, J. Bang, J. Park, S. Kim, S.-M. Park, *Chem. Mater.* **2010**, *22*, 5636.
[22] F. M. Gómez-Campos, M. Califano, *Nano Lett.* **2012**, *12*, 4508.
[23] K. Žídek, K. Zheng, C. S. Ponseca, M. E. Messing, L. R. Wallenberg, P. Chábera, M. Abdellah, V. Sundström, T. Pullerits, *J. Am. Chem. Soc.* **2012**, *134*, 12110.
[24] a) A. Luque, A. Martí, A. J. Nozik, *MRS Bull.* **2007**, *32*, 236; b) R. D. Schaller, V. M. Agranovich, V. I. Klimov, *Nat. Phys.* **2005**, *1*, 189; c) R. D. Schaller, V. I. Klimov, *Phys. Rev. Lett.* **2004**, *92*, 186601; d) R. D. Schaller, M. Sykora, J. M. Pietryga, V. I. Klimov, *Nano Lett.* **2006**, *6*, 424.
[25] M. T. Trinh, A. J. Houtepen, J. M. Schins, T. Hanrath, J. Piris, W. Knulst, A. P. L. M. Goossens, L. D. A. Siebbeles, *Nano Lett.* **2008**, *8*, 1713.
[26] Y. Kanai, J. C. Grossman, *Nano Lett.* **2008**, *8*, 908.
[27] Y. Kanai, J. C. Grossman, *Nano Lett.* **2007**, *7*, 1967.
[28] A. L. Rogach, *Nano Today* **2011**, *6*, 355.
[29] K. Zheng, K. Žídek, M. Abdellah, N. Zhu, P. Chábera, N. Lenngren, Q. Chi, T. Pullerits, *J. Am. Chem. Soc.* **2014**, *136*, 6259.
[30] P. Song, Y. Li, F. Ma, T. Pullerits, M. Sun, *J. Phys. Chem. C* **2013**, *117*, 15879.
[31] D. R. Pernik, K. Tvrdy, J. G. Radich, P. V. Kamat, *J. Phys. Chem. C* **2011**, *115*, 13511.
[32] M. Abdellah, K. Žídek, K. Zheng, P. Chábera, M. E. Messing, T. Pullerits, *J. Phys. Chem. Lett.* **2013**, *4*, 1760.